Earth and Planetary Science Letters 578 (2022) 117329

Contents lists available at ScienceDirect

Earth and Planetary Science Letters

www.elsevier.com/locate/epsl

# Radiative thermal conductivity of single-crystal bridgmanite at the core-mantle boundary with implications for thermal evolution of the Earth

Motohiko Murakami [a,*], Alexander F. Goncharov [b], Nobuyoshi Miyajima [c], Daisuke Yamazaki [d], Nicholas Holtgrewe [b]

[a] Department of Earth Sciences, ETH Zürich, Zürich 8025, Switzerland
[b] Earth and Planets Laboratory, Carnegie Institution of Washington, Washington, DC 20015, USA
[c] Bayerisches Geoinstitut, University of Bayreuth, 95440 Bayreuth, Germany
[d] Institute for Planetary Materials, Okayama University, Misasa, Tottori 682-0193, Japan

ARTICLE INFO

*Article history:*
Received 13 September 2021
Received in revised form 17 November 2021
Accepted 29 November 2021
Available online 8 December 2021
Editor: R. Bendick

*Keywords:*
radiative thermal conductivity of bridgmanite
heat transfer at the core-mantle boundary
thermal history of the Earth

ABSTRACT

The Earth has been releasing vast amounts of heat from deep Earth's interior to the surface since its formation, which primarily drives mantle convection and a number of tectonic activities. In this heat transport process the core-mantle boundary where hot molten core is in direct contact with solid-state mantle minerals has played an essential role to transfer thermal energies of the core to the overlying mantle. Although the dominant heat transfer mechanisms at the lowermost mantle is believed to be both conduction and radiation of the primary lowermost mantle mineral, bridgmanite, the radiative thermal conductivity of bridgmanite has so far been poorly constrained. Here we revealed the radiative thermal conductivity of bridgmanite at core-mantle boundary is substantially high approaching to ~5.3±1.2 W/mK based on newly established optical absorption measurement of single-crystal bridgmanite performed *in-situ* under corresponding deep lower mantle conditions. We found the bulk thermal conductivity at core-mantle boundary becomes ~1.5 times higher than the conventionally assumed value, which supports higher heat flow from core, hence more vigorous mantle convection than expected. Results suggest the mantle is much more efficiently cooled, which would ultimately weaken many tectonic activities driven by the mantle convection more rapidly than expected from conventionally believed thermal conduction behavior.



## 1. Introduction

The evolution of the planet Earth can be ultimately paraphrased as the history of cooling over the past 4.5 billion years since the Earth's surface was fully covered with a deep magma ocean under extremely high-temperature conditions. A number of global dynamics in the Earth including mantle convection, plate tectonics and igneous activities have been driven by huge thermal energies released from deep Earth's interior in the course of this cooling history. This perspective raises the question as to how fast the Earth has been losing heat throughout the Earth's history, which directly links to the fundamental question on how long the Earth will remain dynamically active. To address this issue quantitatively, knowledge of the thermal conductivity of the Earth's deep materials under relevant conditions are obviously essential.

The Earth's core-mantle boundary (CMB) where the solid silicate mantle is in direct contact with the molten iron core is known as the largest thermal boundary in the Earth with significantly steep thermal gradient (Gurnis et al., 1998), which has served as the primary driving force of the mantle dynamics throughout the entire history of the solid Earth (van den Berg et al., 2005; Zhong, 2006; Lay et al., 2008). Since the mixed convection between mantle and core materials is gravitationally prohibited, heat from the hot Earth's core has been believed to be primarily transferred by both conduction ($k_{lat}$, lattice thermal conductivity) and radiation ($k_{rad}$, radiative thermal conductivity) components of the thermal conductivity mechanisms at CMB. Temperature condition just above CMB where the sharp rise in geothermal profile at mantle side is expected has been previously estimated to be ~4100 K (Steinle-Neumann et al., 2001; Deschamps and Trampert, 2004; Manthilake et al., 2011). If this is the case, bridgmanite (Brg) and

* Corresponding author.
*E-mail address:* motohiko.murakami@erdw.ethz.ch (M. Murakami).

https://doi.org/10.1016/j.epsl.2021.117329

ferropericlase (Fp) would be the dominant mineral phases at CMB which are thermodynamically stable under such high-temperature condition in a representative mantle compositional system such as peridotite (Murakami et al., 2005; Hernlund et al., 2005; Tateno et al., 2009). It is thus fundamentally important to clarify the thermal conductivities of those two primary mineral phases at the base of the mantle for unraveling the thermochemical evolution of the Earth.

Previous experimental researches on $k_{lat}$ of both Brg and Fp phases have already been conducted up to CMB pressures at room temperature using diamond anvil cell high-pressure apparatus (DAC) (Ohta et al., 2012, 2017; Hsieh et al., 2018). In addition, the lattice thermal conductivities of Brg and Fp have also been examined recently for the first time under simultaneously high-pressure and high-temperature conditions corresponding to the uppermost lower mantle (Manthilake et al., 2011). Very recently, *in-situ* $k_{lat}$ measurements of Brg and/or post-perovskite phase under high-PT conditions have also been conducted using DAC (Okuda et al., 2020; Geballe et al., 2020). The lattice thermal conductivity values expected from those studies have found to be in good agreement with each other, showing that the peridotitic lower mantle would have $k_{lat}$ around ~8.4-11.0 W/mK at CMB.

Some pioneering experiments on the $k_{rad}$ of Brg and Fp have also been performed under lower mantle pressure conditions at room temperature (Goncharov et al., 2006, 2008, 2010, 2015; Keppler et al., 2008, 2007). The results led to a general consensus that the effect of $k_{rad}$ of Fp on the heat conduction at CMB would be negligibly small due to the high-spin to low-spin transition of iron in Fp at mid-lower mantle pressure condition that significantly enhances its opacity. On the other hand, it still remains highly controversial to what extent $k_{rad}$ of Brg contributes to the heat transfer at CMB. While one experimental study showed almost negligible effect of $k_{rad}$ of Brg below ~0.5 W/mK (Goncharov et al., 2008), the others have estimated $k_{rad}$ of Brg at CMB to be approaching to ~10 W/mK at most (Keppler et al., 2008; Goncharov et al., 2015), which is comparable to the thermal conductivity value at CMB estimated solely from $k_{lat}$ as mentioned above. Due to this huge controversy on $k_{rad}$ of Brg with almost twenty-fold differences among works and the fact that the estimated thermal conductivity from $k_{lat}$ is quite consistent with the conventionally assumed bulk thermal conductivity value at CMB of ~10 W/mK (Lay et al., 2008), the radiative contribution of the thermal conductivity has often been neglected in the previous discussions on the heat conduction at CMB and lattice thermal conductivity has long been regarded as a dominant thermal conductivity mechanism at CMB (Ohta et al., 2012; Manthilake et al., 2011).

However, without proper knowledge on the radiative contribution of the thermal conductivity of Brg at CMB, it is obviously impossible to grasp a complete view of heat conduction behavior at CMB, hence the views on the dynamics and thermochemical evolution in the Earth so far inferred solely from the results of lattice thermal conductivity might be misleading. Although the exact reason for the controversy over the radiative thermal conductivity of Brg (Goncharov et al., 2008, 2015; Keppler et al., 2008) still remains unresolved, one of the critical problems in the previous studies was that all those measurements were performed only under ambient temperature condition and thus they needed to assume that the spectra aren't changed at high $T$ to extrapolate the thermal conductivity under extremely high-temperature condition at CMB, which is not obvious. Serious technical obstacle for such a measurement under high-pressure and high-temperature condition is not only derived from the difficulty to achieve the extreme condition in the lab, but also the problem of the selective chemical segregation (Soret diffusion) potentially induced by a long and inhomogeneous heating method (Sinmyo and Hirose, 2010), which has long prohibited the exploration of the radiative thermal conductivity *in-situ* under high-pressure and high-temperature. Very recently, a groundbreaking experimental work has first shown significantly lower $k_{rad}$ value of 0.35 W/mK at CMB of polycrystalline aggregates in peridotitic system, synthesized *in-situ* in a diamond anvil cell, under simultaneously high-pressure and high-temperature condition corresponding to deep lower mantle (Lobanov et al., 2020).

Another potential issue on the $k_{rad}$ measurements is to properly assess the effect of grain sizes and grain boundaries of the sample that might significantly affect the optical absorption (hence the $k_{rad}$), due to the possible light scattering induced by the lattice disorder/imperfection within the grain boundaries. Because the actual grain size of the lower mantle phases has been believed to be far larger than the mean free path of photons of their phases (Yamazaki et al., 1996, 2000; Kavner and Rainey, 2016), the effect of grain boundaries on $k_{rad}$ should be excluded to discuss the realistic nature of thermal conduction at the deep lower mantle. In that sense, the measurements on polycrystalline aggregates with composite phases might potentially be affected by a number of grain boundaries existing in the sample, and $k_{rad}$ measurement of single-crystal Brg sample would thus be an ideal solution to avoid such ambiguous factors.

To address this issue, we conducted a series of *in-situ* radiative thermal conductivity measurements of iron-bearing single-crystal Brg under simultaneously high-pressure and high-temperature conditions at a pressure of 80 GPa and temperatures up to 2440 K corresponding to the lower part of the lower mantle using recently developed optical absorption measurement system with a short pulsed ultra-bright supercontinuum probe in a pulsed laser-heated DAC (Lobanov et al., 2016, 2017), which enabled the determination of the radiative thermal conductivity of Brg without significant chemical diffusion. The result exhibits excellent agreement with previous predictions that support higher thermal conductivity value (Goncharov et al., 2015), implying the bulk thermal conductivity at CMB expressed as the sum of both radiation and conduction components would become substantially higher than the conventionally assumed value (Lay et al., 2008). This may offer us an entirely new perspective on CMB that is much more thermally and dynamically active than we have so far expected.

## 2. Methods

### 2.1. Synthesis of single-crystal Brg

Synthesis of single-crystal iron-bearing Brg was performed using a Kawai-type high-pressure and high-temperature apparatus by following the thermal gradient method (Shatskiy et al., 2007). We used a stepped $LaCrO_3$ cylindrical heater embedded within a $ZrO_2$ thermal insulation sleeve. The starting oxide mixture of $SiO_2$, MgO and FeO with $Mg(OH)_2$ that was used as a solvent was loaded in a platinum capsule. To achieve the monotonic thermal gradient in the axial direction in the sample chamber, the center of the stepped heater was positioned off-center from the center of the sample capsule, which enhances the crystal growth of the Brg sample. Temperature was monitored using a $W_{97}Re_3/W_{75}Re_{25}$ thermocouple. The sample was first compressed at room temperature to a load of 19 MN (corresponding to 24 GPa), and then heated from 800 to 1350 °C for 4 minutes, and subsequently heated from 1350 °C to 1450 °C for ~1 minutes. The temperature was maintained at 1450 °C for 40 minutes within 5 °C fluctuation, and then quenched to a room temperature. Shatskiy et al., 2007 reported that the chemical impurity of $H_2O$ in the synthesized $MgSiO_3$ Brg with almost the same procedure as ours was as low as 0.014 wt%. The major chemical composition of the synthesized single-crystal Brg was determined to be $(Mg_{0.93},Fe_{0.07})SiO_3$ by the electron microprobe analysis.

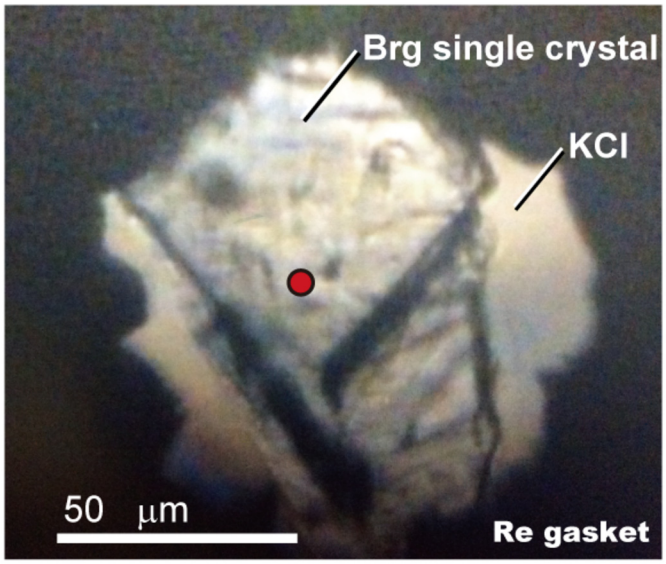


**Fig. 1.** Photomicrograph of the single-crystal bridgmanite sample at 80 GPa in the diamond anvil cell. Red circle indicates the position and spot size (~5 μm) for the optical absorption measurement. As is clearly shown, sufficient spatial dimensions for sample and reference (KCl region) measurements were secured. (For interpretation of the colors in the figure(s), the reader is referred to the web version of this article.)

### 2.2. Optical absorption measurement in a double-sided laser heated DAC

We applied the double-sided laser heating system in a DAC for high-$PT$ optical measurement based on the optical configurations described elsewhere (Lobanov et al., 2016, 2017). A doubly polished thin pellet of the single-crystal Brg shaped by the focused ion beam micromachining (FIB) was loaded into a DAC with 200 μm beveled-culets with KCl pellets which serve as both pressure medium and thermal insulator (Fig. 1). Pressure was determined by the diamond Raman method (Akahama and Kawamura, 2006). A 1070 nm quasi-continuous Yt-doped fiber laser was used as the heating laser source. The laser heating spot was ~2 times larger than the size of the probe spot of the absorption measurement (see Fig. 1). Temperature was measured before and after collecting the optical absorption data at an identical laser power and determined based on the emission spectra fitted to the Planck black body function in a range of 500–800 nm with a time resolution of 0.5–2.0 μs. To achieve double-sided temperature measurements, the sample emission during laser heating was captured from both sides simultaneously on the 2-dimensional iCCD detector array

Temperature was measured spectroradiometrically with collection times ranging from 0.1 to 10 s depending on the emission intensity. The optical response of the system was calibrated using a standard white lamp (Optronics Laboratories OL 220C) and the emission spectrum was analyzed using the T-Rax software (http://www.clemensprescher.com/programs/t-rax) to extract the temperature value.

A Leukos Pegasus pulsed supercontinuum laser was used as the intense white light source for optical absorption measurement in visible range from 400 to 2400 nm. Transmitted light through the sample in a DAC was collected by a 300 mm focal length spectrometer with a 300 gr/mm grating and a gated iCCD detector (Andor iStar SR-303i-A). More detailed optical configurations of the measurement system can be found in McWilliams et al., 2015.

At each pressure, absorption spectra through the sample and the reference spectrum through diamond and KCl pressure medium were obtained to assess the change in the optical properties. As can be seen in Fig. 1, sufficient space for reference spectrum measurement was secured in the sample chamber under high pressure. The principal error sources on $k_{\mathrm{rad}}$ are the uncertainty of the sample thickness ($d$) and refractive index ($n$). The combined propagated uncertainty derived the estimated ambiguities in refractive index and sample thickness was estimated as follows (Lobanov et al., 2020): $\sigma_{total} = \sqrt{\sigma_n^2 + \sigma_d^2}$, $\sigma_n$ and $\sigma_d$ are individual contributions of uncertainty in $n$ and $d$ to $k_{\mathrm{rad}}$.

Absorption signals *in-situ* under high-pressure and high-temperature were collected 200 ms after a start of the 1 s laser heating for 10 ms using properly synchronized gated-detector for visible light.

### 2.3. TEM analysis of the recovered Brg sample from DAC experiments

We have conducted TEM analysis to characterize the chemistries of the recovered Brg sample from high-PT absorption measurements by means of laser heated DAC. A site-specific TEM thin foil of the recovered Brg was prepared with a dual-beam (Ga and field emission electron guns) focused ion beam (FIB) milling machine, *FEI Scios*, equipped with a sample-lift-out manipulator system, *FEI Easylift*. The Ga-beam conditions of the trench milling process are 30 kV for the acceleration voltage and 5–30 nA for the beam current. After cleaning the surface of the TEM thin foil by a 1-nA Ga beam, the lamella was lifted out and glued on a TEM grid by the *Easylift* system. The final thinning conditions are 30 kV and 300 pA to obtain an electron transparency.

The TEM observation was performed in a transmission electron microscope (*Philips CM20 FEG with STEM*), operating at 200 kV. The crystal morphology of bridgmanite was examined using bright field (BF) and dark field (DF) images and selected area electron diffraction (SAED). For chemical analysis, Energy Dispersive X-ray Spectroscopy and Electron Energy-Loss Spectroscopy were performed by using spectrometers (EDS, *Noran Vantage* and EELS, *Gatan 666 PEELS*), which are equipped in the TEM. To minimize electron irradiation damage during EDS and EELS measurements, TEM thin foils were cooled to nearly liquid nitrogen temperature (ca. 100 K) in a Gatan cooling stage.

EDS spectra were collected with 60 s live time and were quantified according to the procedure described elsewhere (van Cappellen and Doukhan, 1994). This method corrects for X-ray absorption on the basis of the principle of electroneutrality and requires the quantification of oxygen. The $k$ factors were calibrated, using the parameter-less correction method (van Cappellen, 1990). Fe-$L_{2,3}$ edge energy loss near edge structure (ELNES) spectra were collected in diffraction mode with convergence and collection semi-angles of $\alpha$ = 8 mrad and $\beta$ = 2.7 mrad, an energy dispersion of 0.1 eV channel and 20 s integration time per readout. The energy resolution is around 0.8 eV, measured as the width of the zero-loss peak at half height. Quantification of the Fe-$L_{2,3}$-ELNES followed the procedure described by the previous works (van Aken et al., 1998; van Aken and Liebscher, 2002), using an empirically calibrated universal curve.

## 3. Results

### 3.1. High pressure and high temperature optical absorption of the Brg

Fig. 2 shows the optical absorption spectra obtained from the single-crystal Brg sample in a series of laser heating cycles at 80 GPa both upon heating at temperatures from 2200 K to 2440 K (Fig. 2 A, C and E) and after respective heating at 300 K (Fig. 2 B, D and F). The short-pulsed supercontinuum probe with ultra-high brightness instead of conventionally used halogen light source allowed the collection of 2500 intense pulses for 10 ms and the

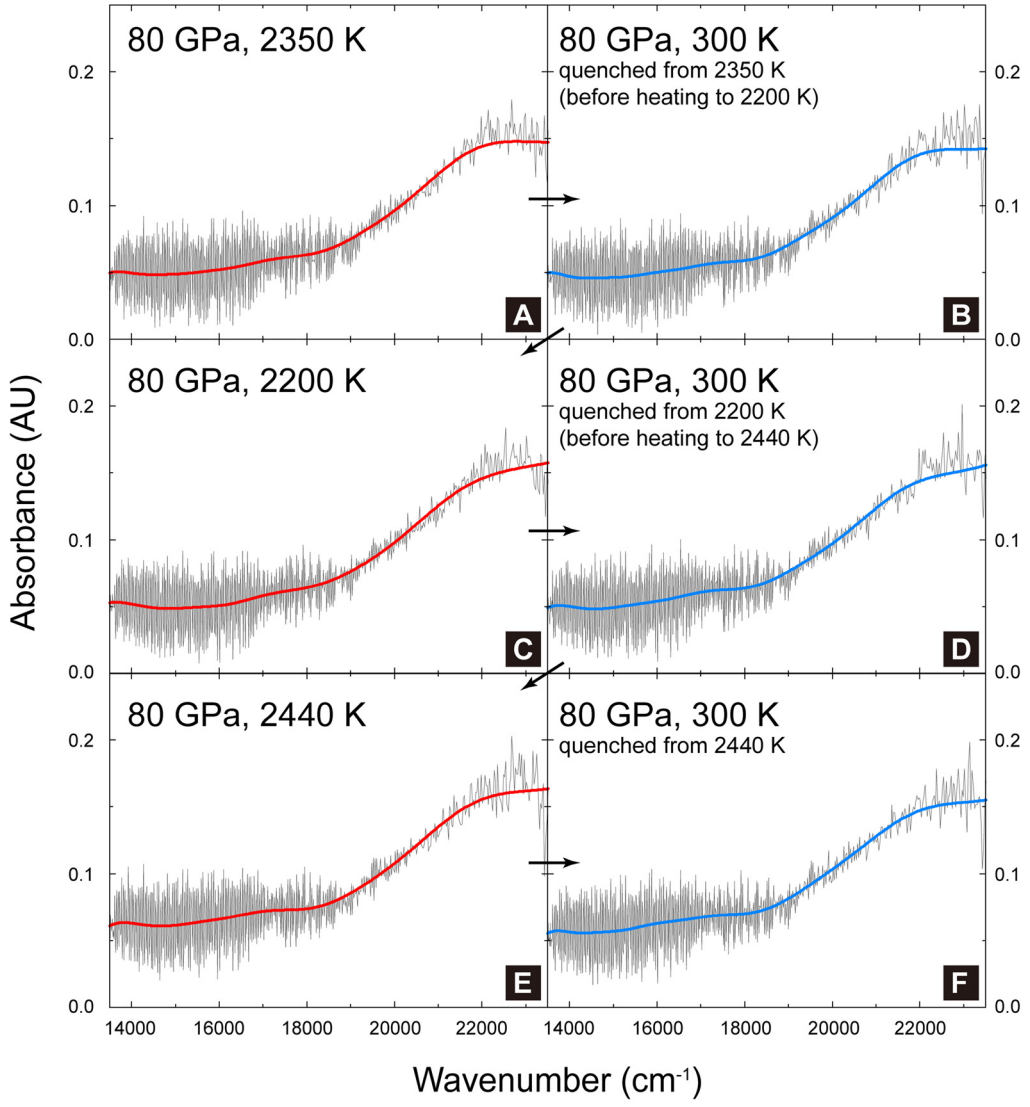


**Fig. 2.** Optical absorption spectra of single-crystal bridgmanite obtained in a series of laser heating cycles both on heating and after heating at 80 GPa. The fitted-trends of absorption spectra are shown in red and blue lines for high-temperature and ambient temperature, respectively, for clarity. **A**, **C**, **E**, absorption spectra upon heating at 2350 K, 2200 K and 2440 K, respectively. **B**, **D**, **F**, absorption spectra after respective heating at 2350 K, 2200 K and 2440 K. The arrows indicate the heating and quenching sequence in this series of experiments. Thus, the spectra shown in B and D can be also considered as the spectra before heating at 2200 K (C) and 2440 K (E), respectively. Absorption coefficient was calculated using $\alpha = A\ln 10/d$, where $A = \log_{10}(I_0/I)$ is the absorbance, $I_0$ and $I$ are the reference measured through the medium at 300 K and sample signals, respectively, and $d$ is the sample thickness determined by measuring the recovered sample during FIB cross sectioning (Fig. 3).

significant suppression of thermal radiation background by several orders of magnitude, which enabled to obtain the high-quality absorption spectrum even under very high temperature for such a short measurement time as shown in Fig. 2. This technical improvement to significantly shorten the measurement time proved to greatly suppress the unwanted selective chemical separation (as discussed later) potentially induced during the laser heating in a DAC (Sinmyo and Hirose, 2010). As can be seen in Fig. 2, we observed almost indistinguishable absorption spectra both before heating and after heating (Fig. 2 B, D and F), which strongly indicates that the short-pulsed laser heating doesn't induce any significant chemical separation upon heating. In addition, the absorption increases very little at high temperatures, suggesting that the temperature effect on $k_{rad}$ due to the modification of the absorption spectrum doesn't significantly change with temperature.

### 3.2. Structure and chemical composition of the recovered Brg

To quantitatively characterize the structure, crystallinity, major element chemistry, and valence state of iron of the recovered Brg sample, the transmission electron microprobe (TEM) analyses with electron diffraction, energy dispersive X-ray spectroscopy (EDS) and electron energy loss spectroscopy (EELS) were conducted for the recovered sample. The precise spot where the optical absorption measurement had been conducted (Fig. 3A) was carefully specified from the recovered sample with *in-situ* FIB observation, and vertical cross section of the Brg sample along the compressional axis of the DAC was prepared for TEM analysis by *in-situ* FIB processing (Fig. 3A). Both bright-field TEM image (Fig. 3B) and selected area electron diffraction pattern (Fig. 3C) clearly show that the recovered single-crystal sample preserved highly crystalline perovskite structure with some fractures, which might be formed by the stresses potentially applied upon decompression. We confirmed fairly homogeneous major element chemistry ($SiO_2$, MgO, and FeO) less than 3% standard deviations throughout the entire sample area we examined in the TEM-EDS mapping (Fig. 3D-F), and determined the chemical composition of the recovered Brg sample to be $(Mg_{0.95},Fe_{0.05})O_3$. Given the chemical composition of Brg before experiments was $(Mg_{0.93},Fe_{0.07})SiO_3$, selective chemi-

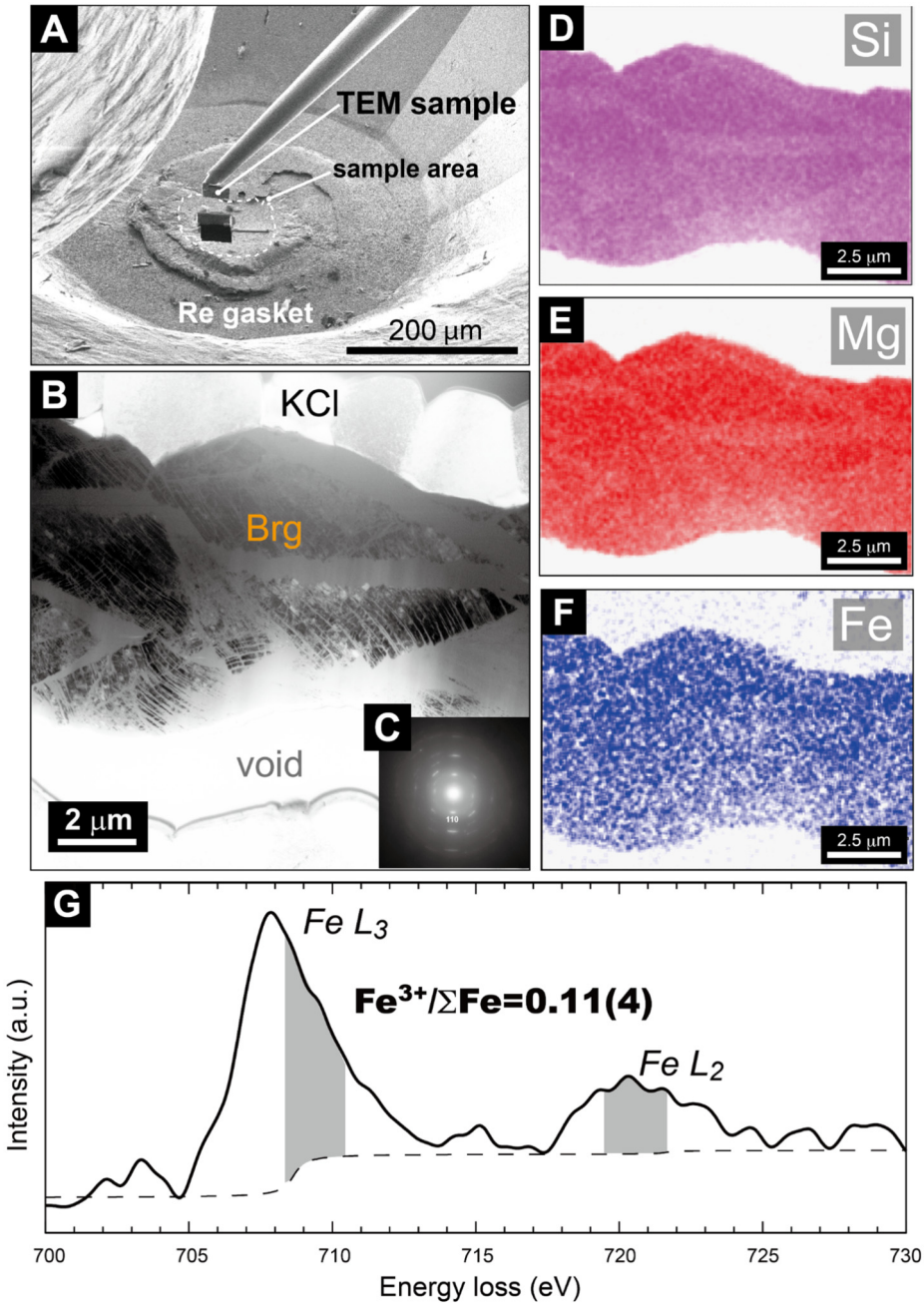


**Fig. 3.** Transmission electron microscopy analysis of the recovered bridgmanite sample. **A**, Focused ion beam scanning electron microscopic (FIB-SEM) image of the recovered diamond anvil cell sample. TEM lamella was extracted parallel to the compressional axis of the diamond anvil cell, which enabled the determination of the sample thickness after recovery. **B**, bright-field TEM image of the bridgmanite (Brg) sample. **C**, selected area electron diffraction pattern of the bridgmanite sample. **D-F**, STEM-EDS (energy dispersive X-ray spectroscopy) mapping for Si, Mg, and Fe, respectively. **G**, TEM-EELS (electron energy loss spectroscopy) data. Fe-$L_{2,3}$ edge energy loss near edge structure (ELNES) of bridgmanite. The areas where we integrated for determining iron valence state are indicated by grey color.

cal separation of iron in our system was found to be suppressed within 2 mol%. The resultant iron content (or Mg#) of the recovered Brg was highly consistent with the plausible chemistry of the Brg in the peridotitic lower mantle (Murakami et al., 2005). Based on the TEM-EELS analysis using integration method (van Aken and Liebscher, 2002), we also determined that the $Fe^{3+}/\Sigma Fe$ ratio in the recovered Brg sample was 0.11(4) (Fig. 3G). Sample thickness at 80 GPa that is an essential parameter to determine the absorption coefficient, which is the main source of uncertainties in $k_{rad}$, was determined to be 6.7 μm (with uncertainties ± ~5%) by the direct thickness measurement of the vertical cross section of the recovered Brg sample (Fig. 3B) with the elastic correction under high-pressure at 80 GPa using an isothermal equation of state (Mao et al., 1991).

### 3.3. Radiative thermal conductivity of the Brg

The radiative thermal conductivity $k_{rad}$ $(T)$ was determined based on the following relation (Goncharov et al., 2008; Keppler et al., 2008):

$$k_{rad}(T) = \frac{4n^2}{3}\int_0^\infty \frac{1}{\alpha(\nu)}\frac{\partial I(\nu, T)}{\partial T}d\nu$$

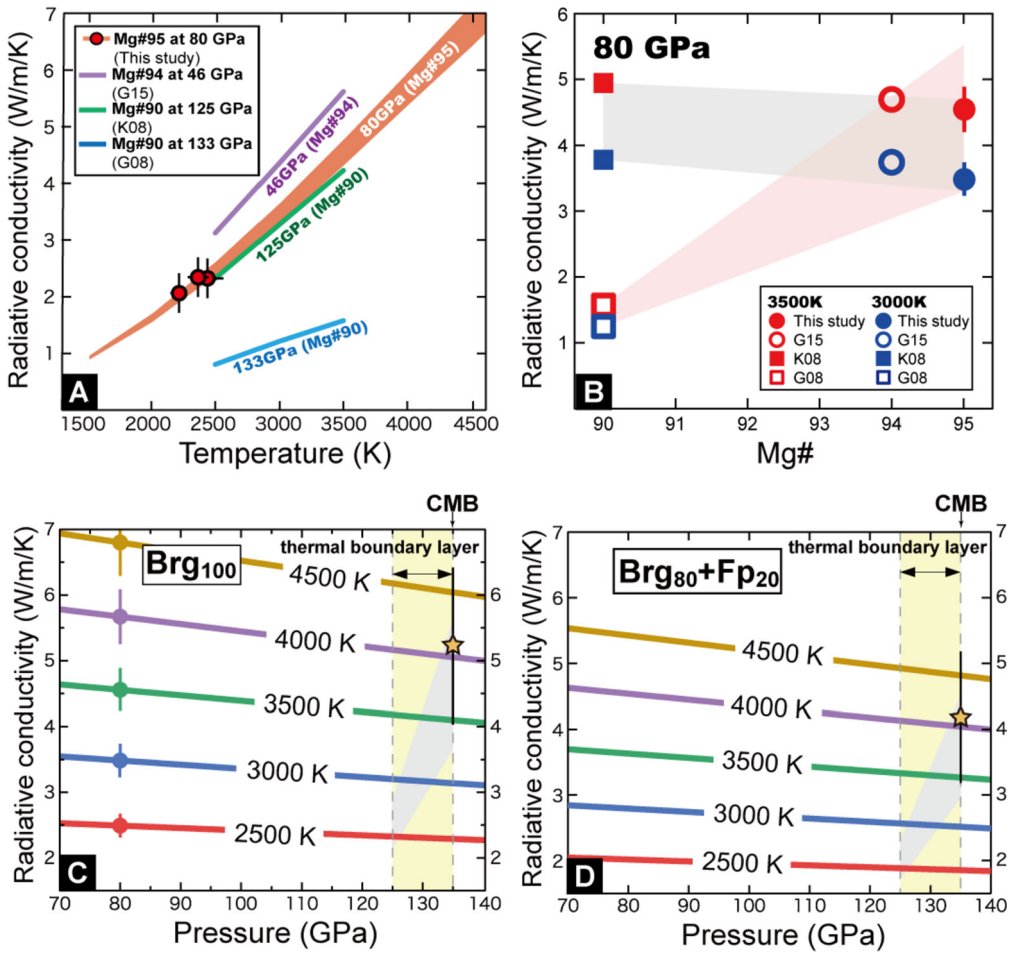


**Fig. 4.** Radiative thermal conductivity of Earth's lower mantle. **A**, radiative thermal conductivity of bridgmanite at 80 GPa and at 2200 K, 2350 K and 2440 K (red points) with its temperature dependence (light red line) determined from the present data. Previous results are also shown in purple (G15, Goncharov et al., 2015), green (K08, Keppler et al., 2008) and blue lines (G08, Goncharov et al., 2008). **B**, radiative thermal conductivities at 80 GPa and at 3000 K and 3500 K as a function of Mg#. Two possible linear trends with Mg# are shown as light grey and light red shaded areas. **C**, **D**, Radiative thermal conductivity of the deep lower mantle for $Brg_{100}$ and $Brg_{80}$ + $Fp_{20}$ models, respectively. Circles shown at 80 GPa in **C** show the fixed $k_{rad}$ values determined from this study. Yellow stars indicate the $k_{rad}$ at the core-mantle boundary at 135 GPa and 4100 K. Grey areas suggest the assumed temperature conditions from the top of D" layer (2600 ±200 K) to its bottom (4100 (+200, -800) K) (Manthilake et al., 2011).

where $n$ is the refractive index, $\nu$ is the frequency, $\alpha$ is the measured absorption coefficient, $I(\nu,T)$ is the Planck function and $T$ is the temperature. Unlike previous results on $k_{rad}$ of Brg, we directly determined the radiative thermal conductivities of Brg simultaneously under high-pressure and high-temperature conditions based on the series of heating experiments at 80 GPa. The refractive index of Brg at 80 GPa was calculated based on a density-correlated theoretical relation (Shannon and Fischer, 2016; Lobanov et al., 2020) (see Supplementary Materials), which creates potential ambiguities of ± ~10 %. The combined propagated error induced by the primary ambiguity sources of thickness and the refractive index to $k_{rad}$ was eventually determined to be ~15 % (see Method).

Fig. 4A shows the $k_{rad}$ values of Brg directly determined in this study at 80 GPa with its temperature dependence calculated based on the fact that absorption spectrum doesn't change with temperature, which was confirmed to be valid in this study to at least 2440 K. We found that the $k_{rad}$ increases monotonously with increasing temperature reaching above ~6.0±0.4 W/mK under CMB temperature condition at ~4100 K. The previous experimental results on single-phase of the Brg are also shown in Fig. 4A (Goncharov et al., 2008, 2015; Keppler et al., 2008). Note that those previous high-pressure experiments were conducted under ambient temperature and the results plotted in Fig. 4A were thus extrapolated to high-temperature by applying the same manner as we did above. While the result by Goncharov et al., 2008 appears to be relatively deviated from others, it is not straightforward to compare them properly from this plot since both the pressure conditions and iron content of the Brg samples are different among those previous works. For better comparison, we thus plotted the $k_{rad}$ values recalculated under the equivalent condition, as a reference, at 80 GPa in pressure and both at 3000 K and 3500 K in temperature as a function of iron contents as shown in Fig. 4B by applying the respective pressure dependence of $k_{rad}$ they previously reported (Goncharov et al., 2008, 2015; Keppler et al., 2008). This plot clearly shows that the $k_{rad}$ values at lower iron contents with Mg# of 94 (Goncharov et al., 2015) and 95 (this study) are fairly high ranging from ~3.5 to ~4.7 W/mK and almost the same with each other merging within experimental errors. On the contrary, the $k_{rad}$ values at higher iron contents with Mg# of 90 (Goncharov et al., 2008; Keppler et al., 2008) are found to be totally incompatible with each other, having more than three times difference in $k_{rad}$ between them. Although it is difficult to give a reasonable explanation for this discrepancy, two respective trends in $k_{rad}$ as a function of iron content can be assumed as shown in Fig. 4B based on those different results, one denoting almost no dependence on iron content (grey shadow in Fig. 4B), and the other with large dependence on iron content increasing $k_{rad}$ nearly three-fold with decreasing the iron content from Mg# 90 to Mg# 94-95 (red shadow in Fig. 4B). It is widely accepted that the $k_{rad}$ of the mineral generally increases with decreasing its iron content due to its

less opacity (Goncharov et al., 2010), and the previous experimental studies have also confirmed that the optical absorbance of Brg measured under ambient condition significantly increases with increasing iron content even from Mg# 95-96 to 90 (Keppler et al., 1994; Goncharov et al., 2008). Taking those facts into account, it might be reasonable to think that the $k_{rad}$ trend with large dependence of iron contents shown as red shadow in Fig. 4B is more preferable though further systematic study would be needed to fully clarify this matter.

## 4. Discussions

### 4.1. Radiative thermal conductivity at the CMB

Since the iron content of the Brg in the plausible lower mantle (e.g., Murakami et al., 2005) with Mg# of ~95 is fairly consistent with that obtained in this study, present experimental results obtained under simultaneously high-pressure and high-temperature should directly place an important constraint on the nature of radiative conductivity in deep lower mantle without any correction derived from the iron contents. It should be noted here again that we safely treat the temperature effect on $k_{rad}$ because we confirmed indistinguishable spectra between ambient and high-temperature conditions (Fig. 2). The fact that we observed almost indistinguishable absorption spectra regardless of temperature conditions could be supported by the theoretical prediction based on the crystal field theory described in Keppler et al., 2008, which indicates the intensity of the absorption spectrum is expected to be nearly independent of temperature possibly due to the site symmetry of $Fe^{2+}$ in Brg located on a distorted dodecahedral site (Kudoh et al., 1990). While the absolute values of $k_{rad}$ among the previous experimental works have exhibited highly divergent as mentioned above, all those previous studies have shown excellent agreement with each other regarding the pressure dependence of $k_{rad}$, which is remarkably small (Goncharov et al., 2008, 2015; Keppler et al., 2008). We thus applied the average pressure dependence/gradient of $k_{rad}$ of those previous works (Goncharov et al., 2008, 2015; Keppler et al., 2008) to model the $k_{rad}$ under deep lower mantle condition, and also applied the temperature dependence of $k_{rad}$ that we determined from a series of heating cycles at 80 GPa as shown in Fig. 4A as the fixed points. On the basis of those pressure and temperature dependence of $k_{rad}$ of Brg, we constructed $k_{rad}$ ($P$, $T$) models for lowermost mantle with both 100% Brg ($Brg_{100}$) and 80% Brg + 20% Fp ($Brg_{80}$+$Fp_{20}$) mineral assemblages in Fig. 4C and D, respectively, provided that the $k_{rad}$ of Fp is negligibly small as previous studies reported (Goncharov et al., 2006; Keppler et al., 2007). Our subsequent estimates of the $k_{rad}$ of both 100% Brg mantle and peridotitic mantle ($Brg_{80}$ + $Fp_{20}$) at CMB condition (135 GPa and 4100 K) were found to be 5.3 ±1.2 W/mK, and 4.2 ±1.0 W/mK, respectively. The discrepancy between the present results using single-crystal and the recent result by Lobanov et al., 2020 showing relatively small $k_{rad}$ using fine polycrystalline aggregates of Brg and Fp synthesized in a DAC is yet to be fully resolved. Although further investigation is essentially required on this issue, grain boundaries might be a key for this discrepancy since it is widely accepted that the grain boundaries in composite phases cause the optical scattering induced by the lattice disorder/imperfection within the grain boundaries or the difference in refractive indices, leading to a significant decrease of $k_{rad}$ (Klemens and Greenberg, 1973). However, again, the fact remains that the effect of grain boundaries of Brg on $k_{rad}$ should be excluded to discuss the realistic nature of radiative thermal conduction at the deep lower mantle since the actual grain size of the Brg has been expected to be far larger than the mean free path of photons of the Brg (Yamazaki et al., 1996, 2000; Kavner and Rainey, 2016).

Although the compositional effect of Al itself in Brg on $k_{rad}$ has been believed to be very limited because an addition of $Al_2O_3$ into Brg changes its transparency very little, possible alteration of ferric-ferrous iron ratio in Brg induced by the incorporation of Al (McCammon, 1997) might affect the $k_{rad}$. Regarding the effect of $Fe^{3+}/\Sigma Fe$ ratio of Brg on its $k_{rad,}$ no reasonable explanation has been successfully given so far for the previous discrepant results on $k_{rad}$ of Brg, for example, between Goncharov et al., 2008 and Keppler et al., 2008 as they both used the Brg samples with almost the same iron content and $Fe^{3+}/\Sigma Fe$ ratio. More importantly, it is still highly controversial issue as to whether Brg phase can really retain high $Fe^{3+}/\Sigma Fe$ ratio under deep lower mantle conditions (Kurnosov et al., 2017; Fu et al., 2018; Mashino et al., 2020), which further makes it difficult to put stronger constraints on this issue. Future systematic experimental investigations on the potential effect of valence state of iron in Brg phase on $k_{rad}$ would thus help to further understand more realistic compositional system of the Earth's lower mantle.

### 4.2. Bulk thermal conductivity at the CMB

Given that previously reported $k_{lat}$ values of $Brg_{80}$+$Fp_{20}$ at CMB are within the range between ~8.4 and ~11.0 W/mK (Manthilake et al., 2011; Ohta et al., 2012; Okuda et al., 2020), expected bulk thermal conductivity at CMB that is the sum of $k_{lat}$ and $k_{rad}$ is approaching to ~15.2 W/mK. This value is above ~1.5 times greater than the widely accepted value estimated based on the geophysical considerations (Lay et al., 2008), which leads us to substantially reconsider the conventional view of nature on heat conduction at CMB. A higher contribution of $k_{rad}$ of Brg to the heat flow would support the view on CMB that is much more thermally and dynamically active than we have so far expected, which should likely stabilize the mantle upwelling rooted in the CMB and help to enhance more vigorous mantle convection. This newly obtained perspective also implies that the Earth's mantle is ~1.5 times more efficiently cooled, which would ultimately weaken many tectonic activities driven by the mantle convection more rapidly than expected from the conventionally believed thermal conduction value (Lay et al., 2008).

### 4.3. Secular change in thermal conductivity at the CMB and the thermal evolution of the Earth

As is obvious from Fig. 4C and D, the $k_{rad}$ in general becomes less with decreasing temperature. Thus, the radiative contribution of the thermal conduction at CMB should be getting smaller with cooling of the mantle. However, the contribution of $k_{lat}$ that increases with temperature instead would sufficiently help to compensate for this loss to keep higher thermal conduction at CMB (Manthilake et al., 2011; Ohta et al., 2012; Okuda et al., 2020). Another important aspect of this issue is to consider the possible change in the stable mantle phases that are in direct contact with the outer core with cooling (decreasing the temperature at CMB). While the major mineral assemblage at CMB under the present CMB temperature condition (~4100 K) (Steinle-Neumann et al., 2001; Deschamps and Trampert, 2004; Manthilake et al., 2011) is expected to be Brg+Fp (Murakami et al., 2005; Tateno et al., 2009) and post-perovskite phase (Ppv) is believed to be present as unevenly distributed lens-like structures just below the D" seismic discontinuity (Hernlund et al., 2005) (Fig. 5A), Ppv should become dominant stable phase at CMB if the temperature at CMB decreases down to one at phase boundary from Brg to Ppv (below ~3500 K) according to the recently reported Clapeyron slope of this phase boundary (Tateno et al., 2009) (Fig. 5B and C). If this is the case, thermal conduction behavior at CMB would change discontinuously along with this possible change in stable phases

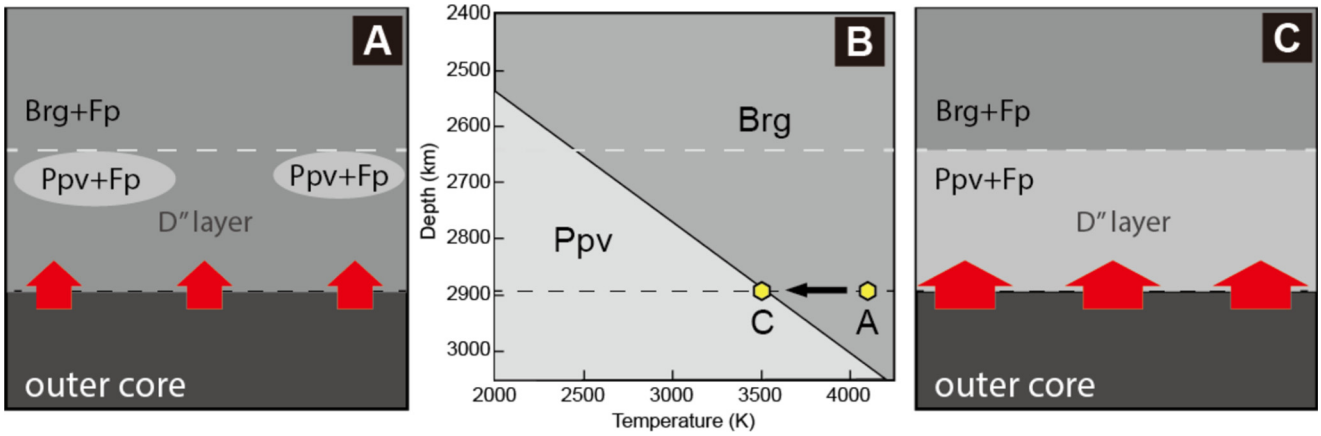


**Fig. 5.** Schematic views on secular change in stable phases and thermal conductivity at core-mantle boundary region. **A**, Schematic cross section of the present CMB region. The dominant phase assemblage at present CMB is Brg and Fp according to the assumed temperature condition at CMB (Manthilake et al., 2011) and phase diagram of $MgSiO_3$ (Tateno et al., 2009) **B**, Phase diagram of $MgSiO_3$ under conditions around D" layer (Tateno et al., 2009). Black and white dashed lines indicate the bottom and top boundary of the D" layer. Yellow symbols with black arrow indicate the possible secular change in temperature at CMB from present (A) to the time when it crosses the phase boundary (C). **C**, Schematic cross section of the future CMB region. Red arrows suggest the schematic magnitude of the thermal conductivity at CMB. When the temperature at CMB decreases down to the phase boundary from Brg to Ppv, the dominant phase which is in direct contact with the outer core would eventually become Ppv. The thermal conductivity at the lowermost mantle thus becomes much higher.

at CMB. Recent pioneering thermal conductivity measurements on Ppv (Ohta et al., 2012; Lobanov et al., 2017: Okuda et al., 2020) indicate that the presence of Ppv at CMB is expected to increase the bulk thermal conductivity ($k_{rad}$+ $k_{lat}$) with significant contribution of $k_{lat}$ (Ohta et al., 2012: Okuda et al., 2020). If we assume the temperature condition below ~3500 K at CMB which stabilizes the Ppv dominantly in the D" layer (Fig. 5C), the expected $k_{lat}$ value at CMB in the peridotitic system becomes greater than ~19-21 W/mK (Ohta et al., 2012: Okuda et al., 2020). Therefore, this discontinuous change in the heat conduction nature at CMB would induce at least ~1.4 times higher bulk thermal conductivity ($k_{rad}$+ $k_{lat}$) than that with the Brg+Fp assemblage (~2 times higher bulk thermal conductivity than the previously accepted value for the current CMB), which would further accelerate the rapid mantle cooling.

## 5. Conclusions

We performed the *in-situ* radiative thermal conductivity measurement of single-crystal bridgmanite using pulsed-laser heated diamond anvil cell under simultaneously high pressure and high temperature conditions corresponding to the deep lower mantle. We observed almost indistinguishable optical spectra both at room temperature and high temperatures up to 2440 K, which confirms that the absorption coefficient increases very little at high temperatures, suggesting that the temperature effect on $k_{rad}$ due to the modification of the absorption spectrum doesn't significantly change with temperature. Our estimates of the $k_{rad}$ of both 100% Brg mantle and peridotitic mantle ($Brg_{80}$ + $Fp_{20}$) at the CMB condition (135 GPa and 4100 K) were found to be 5.3 ±1.2 W/mK, and 4.2 ±1.0 W/mK, respectively. The expected bulk thermal conductivity at CMB that is the sum of $k_{lat}$ and $k_{rad}$ is approaching to ~15.2 W/mK, which is ~1.5 times greater than the widely accepted value estimated based on the geophysical considerations (Lay et al., 2008).

The higher thermal conductivity value at the bottom of the lower mantle than the previously expected value indicates faster heat transfer at the CMB, which would ultimately weaken many tectonic activities driven by the mantle convection more rapidly than expected from the conventionally believed thermal conduction value. The potential emergence of Ppv phase at the CMB in the future would further accelerate the cooling of the mantle.

## CRediT authorship contribution statement

M.M. designed the research conception. M.M., A. G and N. H. performed optical absorption experiments. N.M. conducted TEM analyses. D.Y. synthesized the single-crystal bridgmanite. M.M. wrote the manuscript. All authors discussed the results.

## Declaration of competing interest

The authors declare that they have no known competing financial interests or personal relationships that could have appeared to influence the work reported in this paper.

## Acknowledgements

We thank S. Petitgirard, I. Mashino, A. Shatskiy, N. Tsujino, S. Kamada, S. Ozawa and Y. Ito for their technical assistance for sample synthesis, preparation and characterization. We thank S. Lobanov for help with $k_{rad}$ and $n$ calculations and error analysis. We are grateful to G. Manthilake for his constructive comments. This work was supported by KAKENHI (25247087) and ETH Zürich startup funding to MM. The work at Carnegie was supported by the NSF (Grant Nos. DMR-1039807, EAR/IF-1128867 and EAR-1763287) and Carnegie Institution of Washington. The FIB facility at Bayerisches Geoinstitut is supported by DFG grant INST 91/315-1 FUGG.

## Appendix A. Supplementary material

Supplementary material related to this article can be found online at https://doi.org/10.1016/j.epsl.2021.117329.

## References

Akahama, Y., Kawamura, H., 2006. Pressure calibration of diamond anvil Raman gauge to 310 GPa. J. Appl. Phys. https://doi.org/10.1063/1.2335683.

Deschamps, F., Trampert, J., 2004. Towards a lower mantle reference temperature and composition. Earth Planet. Sci. Lett. https://doi.org/10.1016/j.epsl.2004.02.024.

Fu, S., Yang, J., Zhang, Y., Okuchi, T., McCammon, C., Kim, H., Lee, S.K., Lin, J., 2018. Abnormal elasticity of fe-bearing bridgmanite in the Earth's lower mantle. Geophys. Res. Lett. https://doi.org/10.1029/2018gl077764.

Geballe, Z.M., Sime, N., Badro, J., van Keken, P.E., Goncharov, A.F., 2020. Thermal conductivity near the bottom of the Earth's lower mantle: measurements of pyrolite

up to 120 GPa and 2500 K. Earth Planet. Sci. Lett. https://doi.org/10.1016/j.epsl.2020.116161.
Goncharov, A.F., Haugen, B.D., Struzhkin, V.V., Beck, P., Jacobsen, S.D., 2008. Radiative conductivity in the Earth's lower mantle. Nature 456, 231–234.
Goncharov, A.F., Lobanov, S.S., Tan, X., Hohensee, G.T., Cahill, D.G., Lin, J.-F., Thomas, S.-M., Okuchi, T., Tomioka, N., 2015. Experimental study of thermal conductivity at high pressures: implications for the deep Earth's interior. Phys. Earth Planet. Inter. https://doi.org/10.1016/j.pepi.2015.02.004.
Goncharov, A.F., Struzhkin, V.V., Jacobsen, S.D., 2006. Reduced radiative conductivity of low-spin (Mg, Fe)O in the lower mantle. Science 312, 1205–1208.
Goncharov, A.F., Struzhkin, V.V., Montoya, J.A., Kharlamova, S., Kundargi, R., Siebert, J., Badro, J., Antonangeli, D., Ryerson, F.J., Mao, W., 2010. Effect of composition, structure, and spin state on the thermal conductivity of the Earth's lower mantle. Phys. Earth Planet. Inter. https://doi.org/10.1016/j.pepi.2010.02.002.
Gurnis, M., Wysession, M.E., Knittle, E., Buffett, B.A., 1998. The Core-Mantle Boundary Region. American Geophysical, Union.
Hernlund, J.W., Thomas, C., Tackley, P.J., 2005. A doubling of the post-perovskite phase boundary and structure of the Earth's lowermost mantle. Nature 434, 882–886.
Hsieh, W.-P., Deschamps, F., Okuchi, T., Lin, J.-F., 2018. Effects of iron on the lattice thermal conductivity of Earth's deep mantle and implications for mantle dynamics. Proc. Natl. Acad. Sci. USA 115, 4099–4104.
Kavner, A., Rainey, E.S.G., 2016. Heat transfer in the core and mantle. Deep Earth. https://doi.org/10.1002/9781118992487.ch3.
Keppler, H., Dubrovinsky, L.S., Narygina, O., Kantor, I., 2008. Optical absorption and radiative thermal conductivity of silicate perovskite to 125 gigapascals. Science 322, 1529–1532.
Keppler, H., Kantor, I., Dubrovinsky, L.S., 2007. Optical absorption spectra of ferropericlase to 84 GPa. Am. Mineral. https://doi.org/10.2138/am.2007.2454.
Keppler, H., McCammon, C.A., Rubie, D.C., 1994. Crystal-field and charge-transfer spectra of (Mg, Fe)$SiO_3$ perovskite. Am. Mineral. 79, 1215–1218.
Klemens, P., Greenberg, N., 1973. Radiative heat transfer through composite materials. J. Appl. Phys. https://doi.org/10.1063/1.1662694.
Kudoh, Y., Prewitt, C.T., Finger, L.W., Darovskikh, A., Ito, E., 1990. Effect of iron on the crystal structure of (Mg, Fe)$SiO_3$ perovskite. Geophys. Res. Lett. https://doi.org/10.1029/gl017i010p01481.
Kurnosov, A., Marquardt, H., Frost, D.J., Boffa Ballaran, T., Ziberna, L., 2017. Evidence for a $Fe^{3+}$ rich pyrolitic lower mantle from (Al, Fe)-bearing bridgmanite elasticity data. Nature. https://doi.org/10.1038/nature21390.
Lay, T., Hernlund, J., Buffett, B.A., 2008. Core–mantle boundary heat flow. Nat. Geosci. https://doi.org/10.1038/ngeo.2007.44.
Lobanov, S.S., Holtgrewe, N., Goncharov, A.F., 2016. Reduced radiative conductivity of low spin $FeO_6$-octahedra in $FeCO_3$ at high pressure and temperature. Earth Planet. Sci. Lett. https://doi.org/10.1016/j.epsl.2016.05.028.
Lobanov, S.S., Holtgrewe, N., Ito, G., Badro, J., Piet, H., Nabiei, F., Lin, J.-F., Bayarjargal, L., Wirth, R., Schreiber, A., Goncharov, A.F., 2020. Blocked radiative heat transport in the hot pyrolitic lower mantle. Earth Planet. Sci. Lett. https://doi.org/10.1016/j.epsl.2020.116176.
Lobanov, S.S., Holtgrewe, N., Lin, J.-F., Goncharov, A.F., 2017. Radiative conductivity and abundance of post-perovskite in the lowermost mantle. Earth Planet. Sci. Lett. https://doi.org/10.1016/j.epsl.2017.09.016.
Manthilake, G.M., de Koker, N., Frost, D.J., McCammon, C.A., 2011. Lattice thermal conductivity of lower mantle minerals and heat flux from Earth's core. Proc. Natl. Acad. Sci. https://doi.org/10.1073/pnas.1110594108.
Mao, H.K., Hemley, R.J., Fei, Y., Shu, J.F., Chen, L.C., Jephcoat, A.P., Wu, Y., Bassett, W.A., 1991. Effect of pressure, temperature, and composition on lattice parameters and density of (Fe, Mg)$SiO_3$-perovskites to 30 GPa. J. Geophys. Res. https://doi.org/10.1029/91jb00176.
Mashino, I., Murakami, M., Miyajima, N., Petitgirard, S., 2020. Experimental evidence for silica-enriched Earth's lower mantle with ferrous iron dominant bridgmanite. Proc. Natl. Acad. Sci. USA 117, 27899–27905.
McCammon, C., 1997. Perovskite as a possible sink for ferric iron in the lower mantle. Nature. https://doi.org/10.1038/42685.
McWilliams, R.S., Dalton, D.A., Konôpková, Z., Mahmood, M.F., Goncharov, A.F., 2015. Opacity and conductivity measurements in noble gases at conditions of planetary and stellar interiors. Proc. Natl. Acad. Sci. USA 112, 7925–7930.
Murakami, M., Hirose, K., Sata, N., Ohishi, Y., 2005. Post-perovskite phase transition and mineral chemistry in the pyrolitic lowermost mantle. Geophys. Res. Lett. https://doi.org/10.1029/2004GL021956.
Ohta, K., Yagi, T., Hirose, K., Ohishi, Y., 2017. Thermal conductivity of ferropericlase in the Earth's lower mantle. Earth Planet. Sci. Lett. https://doi.org/10.1016/j.epsl.2017.02.030.
Ohta, K., Yagi, T., Taketoshi, N., Hirose, K., Komabayashi, T., Baba, T., Ohishi, Y., Hernlund, J., 2012. Lattice thermal conductivity of $MgSiO_3$ perovskite and post-perovskite at the core–mantle boundary. Earth Planet. Sci. Lett. https://doi.org/10.1016/j.epsl.2012.06.043.
Okuda, Y., Ohta, K., Hasegawa, A., Yagi, T., Hirose, K., Kawaguchi, S.I., Ohishi, Y., 2020. Thermal conductivity of Fe-bearing post-perovskite in the Earth's lowermost mantle. Earth Planet. Sci. Lett. https://doi.org/10.1016/j.epsl.2020.116466.
Shannon, R.D., Fischer, R.X., 2016. Empirical electronic polarizabilities of ions for the prediction and interpretation of refractive indices: oxides and oxysalts. Am. Mineral. 101, 2288–2300.
Shatskiy, A., Fukui, H., Matsuzaki, T., Shinoda, K., Yoneda, A., Yamazaki, D., Ito, E., Katsura, T., 2007. Growth of large (1 mm) $MgSiO_3$ perovskite single crystals: a thermal gradient method at ultrahigh pressure. Am. Mineral. https://doi.org/10.2138/am.2007.2415.
Sinmyo, R., Hirose, K., 2010. The Soret diffusion in laser-heated diamond-anvil cell. Phys. Earth Planet. Inter. https://doi.org/10.1016/j.pepi.2009.10.011.
Steinle-Neumann, G., Stixrude, L., Cohen, R.E., Gülseren, O., 2001. Elasticity of iron at the temperature of the Earth's inner core. Nature 413, 57–60.
Tateno, S., Hirose, K., Sata, N., Ohishi, Y., 2009. Determination of post-perovskite phase transition boundary up to 4400 K and implications for thermal structure in D″ layer. Earth Planet. Sci. Lett. https://doi.org/10.1016/j.epsl.2008.10.004.
van Aken, P.A., Liebscher, B., 2002. Quantification of ferrous/ferric ratios in minerals: new evaluation schemes of Fe L 23 electron energy-loss near-edge spectra. Phys. Chem. Miner. https://doi.org/10.1007/s00269-001-0222-6.
van Aken, P.A., Liebscher, B., Styrsa, V.J., 1998. Quantitative determination of iron oxidation states in minerals using Fe L 2, 3 -edge electron energy-loss near-edge structure spectroscopy. Phys. Chem. Miner. https://doi.org/10.1007/s002690050122.
van Cappellen, E., 1990. The parameterless correction method in X-ray microanalysis. Microsc. Microanal. Microstruct. https://doi.org/10.1051/mmm:01990001010100.
van Cappellen, E., Doukhan, J.C., 1994. Quantitative transmission X-ray microanalysis of ionic compounds. Ultramicroscopy. https://doi.org/10.1016/0304-3991(94)90047-7.
van den Berg, A.P., Rainey, E.S.G., Yuen, D.A., 2005. The combined influences of variable thermal conductivity, temperature- and pressure-dependent viscosity and core–mantle coupling on thermal evolution. Phys. Earth Planet. Inter. https://doi.org/10.1016/j.pepi.2004.10.008.
Yamazaki, D., Kato, T., Ohtani, E., Toriumi, M., 1996. Grain growth rates of $MgSiO_3$ perovskite and periclase under lower mantle conditions. Science 274, 2052–2054.
Yamazaki, D., Kato, T., Yurimoto, H., Ohtani, E., Toriumi, M., 2000. Silicon self-diffusion in $MgSiO_3$ perovskite at 25 GPa. Phys. Earth Planet. Inter. https://doi.org/10.1016/s0031-9201(00)00135-7.
Zhong, S., 2006. Constraints on thermochemical convection of the mantle from plume heat flux, plume excess temperature, and upper mantle temperature. J. Geophys. Res. https://doi.org/10.1029/2005jb003972.